Monopole and dipole transitions of the cluster states of ^{18}O

T. Baba
Kitami Institute of Technology, 090-8507 Kitami, Japan

M. Kimura
Department of Physics, Hokkaido University, 060-0810 Sapporo, Japan;
Reaction Nuclear Data Centre (JCPRG), Hokkaido University, 060-0810 Sapporo, Japan;
and Research Center for Nuclear Physics (RCNP), Osaka University, 567-0047 Ibaraki, Japan

(Received 28 April 2020; accepted 31 July 2020; published 14 August 2020)

On the basis of an extended antisymmetrized molecular-dynamics calculation, we study the cluster structure of the 0^+ and 1^- states in ^{18}O. We discuss that several different kinds of the cluster states appear in the excitation spectrum, and their monopole and dipole transitions are interesting fingerprints of unique cluster structure. We show that the monopole and dipole transitions are enhanced for the $^{14}\mathrm{C}+\alpha$ cluster states, while they are hindered for the molecular-orbit state. We also point out that a ratio of the electric and isoscalar monopole transition strengths gives a good hint for the structure of the excited states.

DOI: 10.1103/PhysRevC.102.024317

I. INTRODUCTION

The nucleus ^{18}O has been an important testing ground for our understanding of clustering in $N \neq Z$ nuclei. It is of importance and interest to investigate how extra neutrons affect and enrich clustering, since the core nucleus ^{16}O has the famous $^{12}\mathrm{C}+\alpha$ cluster states [1–7].

A number of experimental [8–18] and theoretical [19–26] studies have even explored the $^{14}\mathrm{C}+\alpha$ cluster states in the spectrum of ^{18}O. They firmly established the positive-parity band built on the 0^+_2 state at 3.63 MeV, which has a $^{14}\mathrm{C}(0^+_1)+\alpha$ cluster structure [8,19,20,23–26]. Due to the parity asymmetry of the $^{14}\mathrm{C}+\alpha$ configuration, this band should be accompanied by the negative-parity band (parity doublet). However, the assignment of the negative-parity band has been rather controversial and unsettled. Gai *et al.* [9,10] assigned the 1^-_1 state at 4.46 MeV as the doublet partner of the 0^+_2 state based on the enhanced $E1$ transition strength between them. However, this assignment was not supported by the theoretical calculations [23–26]. For example, from the multiconfiguration cluster model calculations, Descouvemont and Baye [23] pointed out that the 4.46 MeV state is predominated by the $^{14}\mathrm{C}(2^+)+\alpha$ channel and cannot be considered as the partner of the 0^+_2 state. Alternatively, they showed that the calculated 1^-_3 state has the pronounced $^{14}\mathrm{C}(0^+_1)+\alpha$ cluster structure and tentatively assigned it to the 1^- state observed at 7.62 MeV [8,27]. Later, this assignment was corrected by several experiments [13,14]. They assigned a new negative-parity band built on the 1^- state at 8.03 MeV as the partner of the 0^+_2 state. A confusing fact is that this assignment was again denied by another recent experiment: Avila *et al.* [17] reported that the α spectroscopic factor of the 8.03 MeV state is not large, and, hence, the state cannot be a $^{14}\mathrm{C}(0^+_1)+\alpha$ cluster state.

In addition to the $^{14}\mathrm{C}+\alpha$ cluster states, von Oertzen *et al.* [16] proposed a novel type of cluster state which is composed of the $^{12}\mathrm{C}+\alpha$ cluster core and two valence neutrons occupying so-called molecular orbits (MO state). They tentatively assigned the 7.80 and 10.59 MeV states as the 0^+ and 1^- doublet of the MO states. The existence of such MO states was qualitatively supported by antisymmetrized molecular-dynamics (AMD) calculations [26], and experimental efforts to find more convincing evidence is now ongoing [18]. To understand a rich variety of clustering systematics in ^{18}O, we need to identify the pair of the 0^+ and 1^- cluster states.

In this decade, the isoscalar monopole and dipole transition strengths are attracting a lot of interest as a novel probe for the 0^+ and 1^- cluster states, and have already been used for the discussion on clustering in many stable and unstable nuclei [28–45]. Therefore, we expect that they provide a new insight to clustering of ^{18}O.

For this purpose, we perform an extended AMD calculation for ^{18}O taking into account the coupling of the $^{14}\mathrm{C}(0^+_1)+\alpha$ and $^{14}\mathrm{C}(2^+_1)+\alpha$ channels. We analyze the cluster structure of the 0^+ and 1^- states referring their α-spectroscopic factors and investigate how clustering affects the monopole and dipole transition strengths. We show that the dipole transition strength between the doublet of the $^{14}\mathrm{C}+\alpha$ cluster states is greatly enhanced, while that of the MO states is hindered. We also discuss that a ratio of the electric and isoscalar monopole transition strengths also gives us an interesting hint on the cluster structure.

This paper is organized as follows: In the next section, we briefly explain how we calculated the wave functions of the cluster states in ^{18}O. We also explain the electric and isoscalar monopole and dipole transition matrices. In Sec. III, we first review the calculated and observed spectra of the cluster states. Subsequently, we investigate the effect of the

cluster states on patterns of the transition strengths. The final section summarizes this work.

II. THEORETICAL FRAMEWORK

In this study, we use the same Hamiltonian as in our previous study [26],

$$H = \sum_{i=1}^{A} t_i - t_{\text{c.m.}} + \sum_{i<j}^{A} v_{ij}, \tag{1}$$

where t_i and $t_{\text{c.m.}}$ represents the single-particle and center-of-mass kinetic energies. v_{ij} includes the Gogny D1S effective nucleon-nucleon interaction [46] and Coulomb interaction.

The model wave function is a parity-projected Slater determinant,

$$\Phi_{\text{AMD}} = P^{\pi}\mathcal{A}\{\varphi_1, \ldots, \varphi_A\}, \quad \pi = \pm, \tag{2}$$

where P^{π} is the parity-projection operator, and the single-particle wave packet has the deformed Gaussian form [47–49],

$$\varphi_i(\boldsymbol{r}) = \prod_{\sigma=x,y,z} \exp\{-\nu_\sigma(r_\sigma - Z_{i\sigma})^2\} \otimes (\alpha_i|\uparrow\rangle + \beta_i|\downarrow\rangle) \otimes (|p\rangle \text{ or } |n\rangle). \tag{3}$$

Each Gaussian wave packet has the variational parameters; the Gaussian centroid vector $\boldsymbol{Z}_i$ and the spin parameters α_i and β_i. The isospin is fixed to either proton or neutron. The Gaussian width parameters ν_x, ν_y, and ν_z are also the variational parameters and common to all wave packets.

These variational parameters are determined by the following two methods. The first is the energy variation with the constraint, which was already used in our previous study [26]. Using the frictional cooling method, the variational parameters are so chosen to minimize the total energy under the constraint on the quadruple deformation parameter β. We obtain the optimized wave function $\Phi_{\text{AMD}}(\beta)$ for each value of β ($\beta = 0.00, 0.05, \ldots, 1.40$). As discussed in Ref. [26], if β is small, we obtain the almost spherical shell-like wave functions corresponding to the ground state. With the increase of β, we obtain a variety of cluster states such as the $^{14}\text{C}+\alpha$ cluster, molecular-orbit state, and linear chain of α particles.

In this study, we extend a model space by applying the second method. We use Brink-type wave functions which are ^{14}C and α cluster wave functions placed on the z axis with the intercluster distance d,

$$\Phi_{\text{Brink}}(d) = P^{\pi}\mathcal{A}\left\{\Phi_\alpha\left(-\frac{14}{18}d\right)\Phi_{\text{C}}\left(\frac{4}{18}d\right)\right\}. \tag{4}$$

Here, Φ_α and Φ_{C} represents the intrinsic wave functions of ^{4}He and ^{14}C, respectively. Φ_α is assumed to have the $(0s)^4$ configuration, and Φ_{C} is approximated by a single AMD wave function which has 90% overlap with the full GCM wave function obtained in Refs. [50,51]. The intercluster distance d ranges from 0.4 fm to 8.0 fm with the intervals of 0.4 fm. Since Φ_{C} is oblately deformed, we consider three different orientations of ^{14}C cluster. Figures 1(a)–1(c) show the example of the $^{14}\text{C}+\alpha$ Brink wave functions in which the symmetry axis of ^{14}C is directed to the z, x, and y axis, respectively. Note that the superposition of different orientations of Φ_{C} naturally handles the coupling of $^{14}\text{C}(0_1^+)+\alpha$ and $^{14}\text{C}(2_1^+)+\alpha$ channels, which is known to be important in describing the $^{14}\text{C}+\alpha$ cluster [23]. This point is an advantage of the present calculation compared with previous AMD studies.

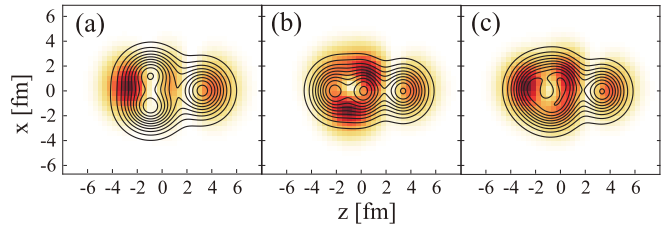

FIG. 1. Density distributions of the Brink-type wave functions in which the symmetry axis of the oblately deformed ^{14}C is directed along the (a) z, (b) x, and (c) y axis. The intercluster distance d is fixed at 4.8 fm in all panels.

These wave functions are projected to the eigenstate of the angular momentum and are superposed to describe the ground and excited states,

$$\Psi^{J^\pi}_{Mp} = \sum_{Ki} f_{Kip} P^J_{MK} \Phi^\pi_{\text{AMD}}(\beta_i) + \sum_{Ki} g_{Kip} P^J_{MK} \Phi^\pi_{\text{Brink}}(d_i), \tag{5}$$

where P^J_{MK} and the index p denote the angular-momentum projection operator and quantum numbers other than the angular momentum, respectively. The coefficients f_{Kip} and g_{Kip} are determined by diagonalizing the Hamiltonian [52].

As a measure of the $^{14}\text{C}+\alpha$ clustering, we calculate the α-spectroscopic factor. We first calculate the α reduced width amplitude (RWA) which is the probability amplitude to find the ^{14}C and α clusters at the intercluster distance a. It is defined as the overlap between the reference cluster state and the wave function given by Eq. (5),

$$y_{j\ell J}(a) = \sqrt{\frac{18!}{14!4!}}\left\langle \frac{\delta(r-a)}{r^2}\Phi_\alpha\left[\Phi^j_{\text{C}}Y_\ell(\hat{r})\right]^J_M \middle| \Psi^{J\pi}_{Mp}\right\rangle, \quad j = 0^+ \text{ or } 2^+. \tag{6}$$

The reference cluster state (bra state) is the $^{14}\text{C}(j)+\alpha$ cluster state in which the $^{14}\text{C}(j)$ and α clusters are mutually orbiting with intercluster distance a, and the intrinsic angular momentum j of the ^{14}C cluster is coupled with the orbital angular momentum ℓ to the total angular momentum J. Here, the α-cluster wave function Φ_α is the same as what appears in Eq. (4), while the ^{14}C cluster wave function Φ^j_{C} is projected to the eigenstate of the angular momentum $j^\pi = 0^+$ or 2^+ from the intrinsic wave function Φ_{C} in Eq. (4). In the practical calculation, Eq. (6) is evaluated by the Laplace expansion method [53]. The α spectroscopic factor S_α is given by a squared integral of $y_{j\ell J}$,

$$S_\alpha = \int_0^\infty daa^2|y_{j\ell J}(a)|^2. \tag{7}$$

In this work, we focus on the electric and isoscalar monopole ($E0$ and $IS0$) and dipole ($E1$ and $IS1$) transition

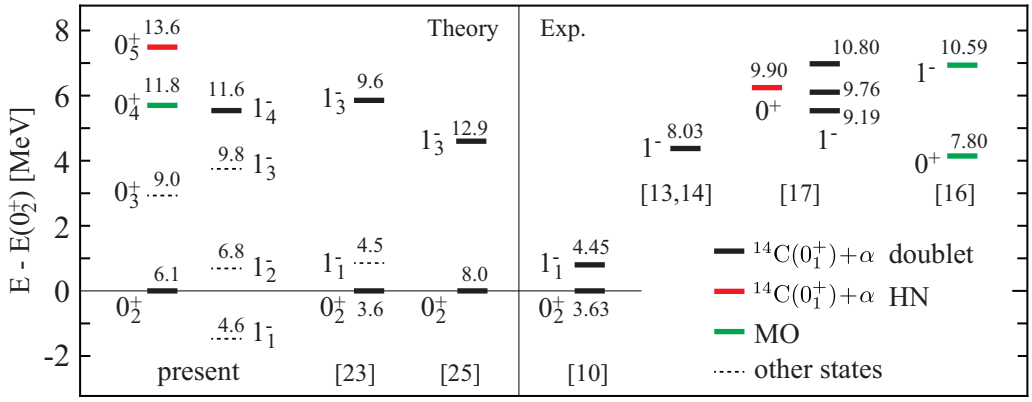

FIG. 2. Spectrum of the 0^+ and 1^- states obtained by the present calculation in comparison with other model calculations [23,25]. Vertical axis shows the energy relative to the 0_2^+ state, while numbers in the figure show the energies relative to the ground state. The proposed assignments of the cluster states 1^- (0^+) with cluster configurations based on the experiments [8,10,13,14,16,17,27] are also shown.

strengths. As discussed in Refs. [9,10], the $E1$ transition strength is a good probe for the $^{14}\mathrm{C}+\alpha$ cluster states, since the intrinsic structure has a static dipole moment. In addition to the $E1$ transition strength, in this decade, the $E0$, $IS0$, and $IS1$ transition strengths have been regarded and utilized as a novel probe for the various kinds of clustering [31,39], as it was proved that these transitions from the ground state to an excited cluster state must be considerably enhanced. The transition operators are defined as follows:

$$\mathcal{M}^{E0} = \sum_{i=1}^{Z} e r_i'^2, \quad \mathcal{M}^{IS0} = \sum_{i=1}^{A} r_i'^2, \tag{8}$$

$$\mathcal{M}^{E1}_{\mu} = \sum_{i=1}^{Z} e r_i' Y_{1\mu}(\hat{r}_i'), \quad \mathcal{M}^{IS1}_{\mu} = \sum_{i=1}^{A} r_i'^3 Y_{1\mu}(\hat{r}_i'). \tag{9}$$

Note that the single-particle coordinate $\boldsymbol{r}_i'$ is measured from the center-of-mass $\boldsymbol{r}_{\mathrm{c.m.}}$, i.e., $\boldsymbol{r}_i' \equiv \boldsymbol{r}_i - \boldsymbol{r}_{\mathrm{c.m.}}$, and hence, our calculation is free from the spurious center-of-mass contributions. The transition strength from the initial state $\Psi_{0p}^{J^\pi}$ to the 0^+ state is evaluated by the reduced transition matrix,

$$M(\lambda; J^\pi \to 0^+) = \langle \Psi^{0^+} | \mathcal{M}_0^\lambda | \Psi_{0p}^{J^\pi} \rangle, \tag{10}$$

where $\mathcal{M}_0^\lambda$ is any of the transition operators where λ is either $E0$, $IS0$, $E1$, or $IS1$.

III. RESULTS

A. Cluster states and their structure

Figure 2 shows spectra of the 0^+ and 1^- states obtained by the present calculation compared with the other theoretical calculations [23,25]. It also shows the proposed assignments of the cluster states based on the experiments [8,10,13,14,16,17,27]. The ground state does not have a pronounced cluster structure but a slightly deformed shell-like structure shown in Fig. 3(a). As explained in our previous work [26], this state is dominated by the neutron $(d_{5/2})^2$ configuration, although the density distribution of the two valence neutrons is similar to that of the Nilsson orbit ([220, 1/2]) due to non-negligible quadrupole deformation.

In the present calculation, the bandhead of the positive-parity $^{14}\mathrm{C}(0_1^+)+\alpha$ cluster band is obtained as the 0_2^+ state at 6.1 MeV, which slightly overestimates the observed excitation energy (3.63 MeV). From the calculated spectroscopic factor shown in Fig. 4, this assignment is rather unique because only this state is dominated by the $^{14}\mathrm{C}(0_1^+)+\alpha$ channel in the low-energy region. It is interesting to note that the intrinsic density of this state shown in Fig. 3(b) does not clearly show the α clustering despite of its large α spectroscopic factor, but it looks like a strongly deformed state. Indeed, it has a 1.7:1 ratio of the large axis over the small axis and a $2\hbar\omega$ excited single-particle configuration. Therefore, this state may also be regarded as a superdeformed state. We consider that this state has duality of superdeformation and clustering. Note that such duality has also been discussed for various nuclei by many authors [54–61].

The corresponding negative-parity partner is also uniquely identified as the 1_4^- state at 11.6 MeV. It is clear that other 1^- states have relatively small spectroscopic factors and are excluded from the doublet partner. For example, the intrinsic density of the 1_1^- state [Fig. 3(e)] clearly shows the absence

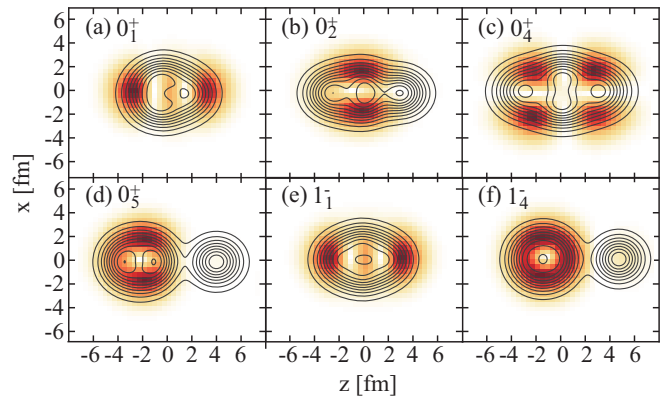

FIG. 3. Density distributions of the intrinsic states which are the dominant component of each 0^+ or 1^- state. Solid lines show the proton density distribution, while the color plot show that of two valence neutrons.

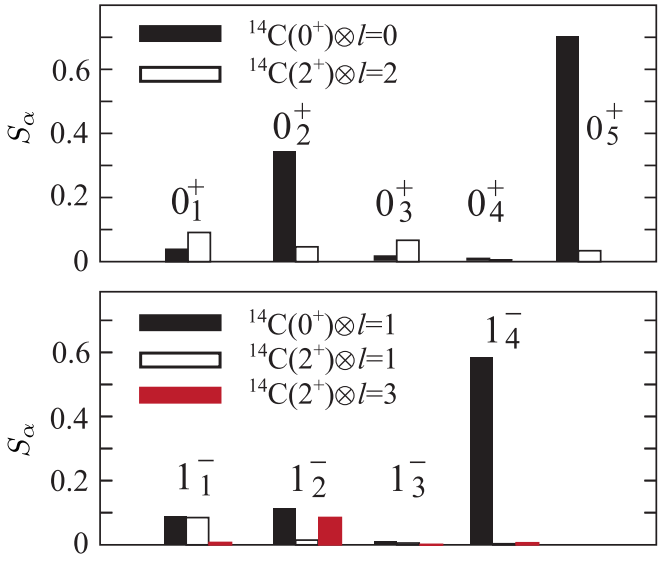

FIG. 4. Calculated α spectroscopic factors of the 0^+ and 1^- states.

of the prominent α clustering in this state. Thus, the present calculation yields 5.5 MeV energy splitting between the 0^+ and 1^- doublet of the $^{14}\mathrm{C}(0^+_1)+\alpha$ configuration, which is larger than that of the $^{12}\mathrm{C}+\alpha$ doublet of ^{16}O (3.5 MeV), and as large as that of the $^{16}\mathrm{O}+\alpha$ doublet of ^{20}Ne (5.9 MeV). This indicates a distortion of the $^{14}\mathrm{C}(0^+_1)+\alpha$ clustering in the positive-parity state which brings about extra binding energy to the 0^+ state and enlarges the doublet splitting. It is notable that other theoretical calculations also yielded similar magnitudes of the splitting: Furutachi *et al.* [25] reported the 4.9 MeV splitting from their AMD calculation which used a different effective interaction and model wave functions from ours. Descouvemont *et al.* [23] reported 6.0 MeV splitting from their multiconfiguration cluster model calculation. Thus, theoretical calculations suggest the consistent magnitudes of the doublet splitting approximately equal to 5–6 MeV.

Experimentally, the assignment of the positive-parity $^{14}\mathrm{C}(0^+_1)+\alpha$ state is well established and unique [8,19,20,23–26]; it is the 0^+_2 state at 3.63 MeV, but the assignment of the negative-parity state is controversial. Gai *et al.* [10] proposed the 1^-_1 state at 4.45 MeV as the partner of the 0^+_2 state because the $^{14}\mathrm{C}+\alpha$ intrinsic structure can naturally explain the observed strong $E1$ transition between them. However, this assignment gives a very small doublet splitting of 0.82 MeV, which contradicts to all theoretical calculations. Furthermore, the present calculation shows the 1^-_1 state is a mixture of the small amount of the $^{14}\mathrm{C}(0^+_1)+\alpha$ and $^{14}\mathrm{C}(2^+_1)+\alpha$ components, which is consistent with the results by Descouvemont *et al.* [23] but contradicts the assignment by Gai *et al.* Other candidates of the doublet partner are the 1^- state at 8.03 MeV observed by the breakup reaction [13,14] and the 9.19, 9.76, and 10.39 MeV states observed by the resonant scattering [17]. In these assignments, the magnitudes of the doublet splitting are approximately in between 4 to 7 MeV. Thus, all these assignments look compatible with the theoretical results, but there is no conclusive evidence.

TABLE I. Calculated reduced matrix for the $E0$, $IS0$, $E1$, and $IS1$ transitions in Weisskopf units (in 10^{-2} W.u. for the $E1$ transitions). 1 W.u. is equal to 5.93 $e\,\mathrm{fm}^2$, 5.93 fm^2, 0.665 $e\,\mathrm{fm}$, and 4.39 fm^3 for the $E0$, $IS0$, $E1$, and $IS1$ transitions, respectively.

$J^\pi_i \to J^\pi_f$	M^{E0} [W.u.]	M^{IS0} [W.u.]
$0^+_1 \to 0^+_2$	0.36	0.67
$0^+_1 \to 0^+_3$	0.28	0.83
$0^+_1 \to 0^+_4$	0.02	0.02
$0^+_1 \to 0^+_5$	0.28	0.56
$0^+_2 \to 0^+_5$	1.31	2.75
	M^{E1} [10^{-2} W.u.]	M^{IS1} [W.u.]
$1^-_1 \to 0^+_1$	1.20	0.77
$1^-_2 \to 0^+_1$	2.53	0.51
$1^-_3 \to 0^+_1$	7.99	0.40
$1^-_4 \to 0^+_1$	3.57	0.70
$1^-_1 \to 0^+_2$	5.11	1.58
$1^-_2 \to 0^+_2$	7.23	1.74
$1^-_3 \to 0^+_2$	2.94	0.75
$1^-_4 \to 0^+_2$	17.3	5.19
$1^-_4 \to 0^+_5$	38.7	17.4

In addition to the $^{14}\mathrm{C}+\alpha$ doublet, the present calculation predicts two excited cluster states; the 0^+ states at 11.8 MeV (0^+_4) and 13.6 MeV (0^+_5) whose intrinsic densities are shown in Figs. 3(c) and 3(d), respectively. The 11.8 MeV state has the $^{12}\mathrm{C}+\alpha$ cluster core surrounded by the valence neutrons occupying the molecular orbit (MO state) which is similar to those known for Be, C, and Ne isotopes [50,62–66]. We consider that this state may correspond to the MO structure suggested by von Oertzen, who proposed a tentative assignment to the 7.80 MeV state [16]. The 0^+_5 state at 13.6 MeV is the $^{14}\mathrm{C}+\alpha$ higher-nodal state (HN state). In this state relative motion between the ^{14}C and α clusters is excited as seen in its density distribution [Fig. 3(d)]. The corresponding observed state might be the 9.90 MeV state reported by Avila *et al.* [17], because it is the only 0^+ state which has a large spectroscopic factor in this energy region.

In short, theoretical calculations predict the doublet of the 0^+ and 1^- states with the $^{14}\mathrm{C}+\alpha$ configuration, but the assignment of the 1^- state has not been established uniquely. The $^{14}\mathrm{C}+\alpha$ HN and MO states are also suggested by the experiments and the present calculation.

B. Monopole and dipole transitions to and between the cluster states

Here, we investigate how the characteristics of the cluster states discussed in the previous section are reflected to the $E0$, $IS0$, $E1$, and $IS1$ transition strengths listed in Table I. For this purpose, the calculated transitions are schematically illustrated in Fig. 5.

In Ref. [31], Yamada *et al.* proved that electric and isoscalar monopole transitions from the ground state to the α-cluster state can be considerably enhanced. Since the α-

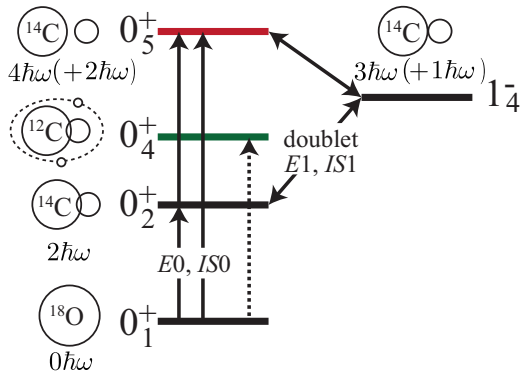

FIG. 5. Schematic figure which illustrates the cluster states of ^{18}O and the transitions among them.

cluster states appear at relatively small excitation energy compared with other collective states [67], the strong $E0$ and $IS0$ strengths at small excitation energy can be attributed to the α-cluster formation. Therefore, the strong monopole transition has been regarded as a signature of the cluster states in stable and unstable nuclei [28–38,41,44,45]. In the present calculation, as expected, we find that the 0^+_2 state, which has a $^{14}\mathrm{C}+\alpha$ cluster structure, has nonsmall $E0$ and $IS0$ transition strengths from the ground state. However, they are not as strong as the Weisskopf unit for the following reason: As seen in Fig. 4 and also discussed in Ref. [23], the dominant cluster component of the ground state is the $^{14}\mathrm{C}(2^+_1)+\alpha$ channel, while that of the 0^+_2 state is different, the $^{14}\mathrm{C}(0^+_1)+\alpha$ channel. This mismatch of the internal structure reduces the monopole strengths between them. The same argument also applies to the 0^+_5 state. As the 0^+_5 state is also dominated by the $^{14}\mathrm{C}(0^+_1)+\alpha$ channel, the monopole transition from the ground state is not so enhanced. On the contrary, the transition between the 0^+_2 and 0^+_5 states is very strong because they have similar internal structure. It is interesting to note that the $IS0$ matrices for the $0^+_1\to 0^+_2$ and $0^+_1\to 0^+_5$ transitions are almost twice as large as the $E0$ matrices. This is naturally understood because these excitations are α clustering, and, hence, protons and neutrons should contribute equally to the transitions. On the other hand, for the $0^+_1\to 0^+_3$ transition, the $IS0$ matrix is much larger than twice of the $E0$ matrix. This is due to the fact that the 0^+_3 state is not an α-cluster state but an excited state predominated by the excitation of valence neutrons. Thus, not only the magnitude but also the ratio of the electric and isoscalar monopole matrices gives us an insight to nuclear structure. We also note that the $0^+_1\to 0^+_4$ transition is rather hindered in both of the electric and isoscalar channels compared with other states because the 0^+_4 has a MO structure so that the $0^+_1\to 0^+_4$ transition involves the rearrangement of the two valence neutrons. A similar hindrance of the monopole transitions was also discussed for Be isotopes [32,36].

Experimentally, two different values of $M(E0)$ for the $0^+_1\to 0^+_2$ transition were reported: The lower value of 0.49 W.u. is not far from our result, but the larger value of 1.01 W.u. is much larger than ours. There is a possibility that we underestimated the α clustering of the 0^+_2 state. In particular, the amount of the $^{14}\mathrm{C}(2^+)+\alpha$ component in the 0^+_2 state may not be large enough in our calculation because the transition strength is sensitive to it. We also mention the importance of the rotational effect of the ^{14}C cluster. If we calculate the $0^+_1\to 0^+_2$ transition without the $^{14}\mathrm{C}+\alpha$ Brink-basis wave functions, the electric monopole transition strength is 0.18 W.u., which is much smaller than both of the experimental values. As for the $0^+_1\to 0^+_{4,5}$ transitions, no corresponding experimental data have been reported so far. The measurement of the transition strengths from the ground states to the 7.80 and 9.90 MeV states will provide an interesting hint about clustering in ^{18}O, as they are the candidates of the calculated $0^+_{4,5}$ states.

The electric and isoscalar dipole transitions are good probes to identify the 1^- cluster states because they are enhanced between the doublet (0^+ and 1^- states) [9,39]. Indeed, the present results confirm that both of the electric and isoscalar dipole transition matrices are large for the $1^-_4\to 0^+_2$ transition. Furthermore, we find that they are also enhanced for the $1^-_4\to 0^+_5$ transition because of the well-developed cluster structure of the 0^+_5 state. Experimentally, the 8.03, 9.19, 9.76, and 10.39 MeV states are the candidates of the 1^-_4 state, which constitutes the doublet with the 0^+_2 state, but the convincing evidence is missing. Therefore, the magnitude of the dipole transitions of these candidates will be very useful to identify the doublet.

Compared with the $1^-_4\to 0^+_2$ transition, the $1^-_4\to 0^+_1$ transition is not so enhanced. This may be again due to the mismatch of the internal structure. The ground state is dominated by the $^{14}\mathrm{C}(2^+_1)+\alpha$ channel, while the 1^-_4 state is dominated by the $^{14}\mathrm{C}(0^+_1)+\alpha$ channel. We note that a similar discussion was also made for the $1^-_2\to 0^+_1$ transition of ^{16}O [43]. Finally, we mention the $1^-_1\to 0^+_2$ transition for which a very strong $E1$ transition was reported by Gai *et al.* In our calculation, like other theoretical calculations, the enhanced $E1$ transition was not reproduced because the 1^-_1 state exhibits no clustering, as seen in its density [Fig. 3(e)]. This may indicate that some cluster correlations are missing in theoretical calculations. Thus, the inconsistency between the theory and experiment for the 1^-_1 state still remains an open question.

IV. SUMMARY

To understand clustering systematics in a $N\neq Z$ nucleus ^{18}O, we perform an extended AMD calculation, taking into account the coupling of the $^{14}\mathrm{C}(0^+_1)+\alpha$ and $^{14}\mathrm{C}(2^+_1)+\alpha$ channels, and analyzed the cluster structure of the 0^+ and 1^- states. We also investigate to what extent the characteristics of the cluster states are reflected in the patterns of the monopole and dipole transition strengths.

Based on the calculated α spectroscopic factors, we identify the 0^+_2 and 1^-_4 states as a doublet of the $^{14}\mathrm{C}(0^+_1)+\alpha$ cluster states. This assignment gives 5.5 MeV for the doublet splitting, which is consistent with other theoretical calculations. Furthermore, our calculation predicts the 0^+_4 and 0^+_5 states, which respectively have the MO structure and the $^{14}\mathrm{C}(0^+_1)+\alpha$ HN structure.

From the analysis of the electric and isoscalar monopole transitions, we find that the transitions to the $^{14}C + \alpha$ cluster states, namely, the $0_1^+ \to 0_2^+$ and $0_1^+ \to 0_5^+$ transitions, are much stronger than the transition to the MO state ($0_1^+ \to 0_4^+$). This is a good measure to distinguish the $^{14}C + \alpha$ cluster states and MO states and to identify an experimental counterpart of the 0_5^+ state. We also find that, for the $0_1^+ \to 0_2^+$ and $0_1^+ \to 0_5^+$ transitions, the isoscalar transition matrix is approximately twice as large as the electric transition matrix reflecting the fact that protons and neutrons equally contribute to these α-clustering excitations.

As for the dipole transitions, we confirm that both electric and isoscalar dipole transitions are greatly enhanced between the $^{14}C + \alpha$ cluster states, namely, the $1_4^- \to 0_2^+$ and $1_4^- \to 0_5^+$ transitions. However, we could not resolve the inconsistency between theories and experiments for the electric-dipole transition of the 1_1^- state.

ACKNOWLEDGMENTS

The authors acknowledge support by the grant for the RCNP joint research project at Osaka University and by the collaborative research program 2019 at Hokkaido University. The numerical calculation was conducted on a supercomputer at Research Center for Nuclear Physics,. One of the authors (M.K.) acknowledges the support by the JSPS KAKENHI Grant No. JP19K03859.

[1] A. Arima, H. Horiuchi, and T. Sebe, Phys. Lett. B **24**, 129 (1967).
[2] H. Horiuchi and K. Ikeda, Prog. Theor. Phys. **40**, 277 (1968).
[3] B. Buck, C. B. Dover, and J. P. Vary, Phys. Rev. C **11**, 1803 (1975).
[4] Y. Suzuki, Prog. Theor. Phys. **55**, 1751 (1976).
[5] Y. Suzuki, Prog. Theor. Phys. **56**, 111 (1976).
[6] Y. Fujiwara, H. Horiuchi, K. Ikeda, M. Kamimura, K. Kato, Y. Suzuki, and E. Uegaki, Prog. Theor. Phys. Suppl. **68**, 29 (1980).
[7] P. Descouvemont, D. Baye, and P. H. Heenen, Nucl. Phys. A **430**, 426 (1984).
[8] A. Cunsolo, A. Foti, G. Immè, G. Pappalardo, G. Raciti, and N. Saunier, Phys. Rev. C **24**, 476 (1981).
[9] Y. Alhassid, M. Gai, and G. F. Bertsch, Phys. Rev. Lett. **49**, 1482 (1982).
[10] M. Gai, M. Ruscev, A. C. Hayes, J. F. Ennis, R. Keddy, E. C. Schloemer, S. M. Sterbenz, and D. A. Bromley, Phys. Rev. Lett. **50**, 239 (1983).
[11] M. Gai, R. Keddy, D. A. Bromley, J. W. Olness, and E. K. Warburton, Phys. Rev. C **36**, 1256 (1987).
[12] M. Gai, S. L. Rugari, R. H. France, B. J. Lund, Z. Zhao, D. A. Bromley, B. A. Lincoln, W. W. Smith, M. J. Zarcone, and Q. C. Kessel, Phys. Rev. Lett. **62**, 874 (1989).
[13] N. Curtis, D. D. Caussyn, C. Chandler, M. W. Cooper, N. R. Fletcher, R. W. Laird, and J. Pavan, Phys. Rev. C **66**, 024315 (2002).
[14] S. Yildiz, M. Freer, N. Soić, S. Ahmed, N. I. Ashwood, N. M. Clarke, N. Curtis, B. R. Fulton, C. J. Metelko, B. Novatski, N. A. Orr, R. Pitkin, S. Sakuta, and V. A. Ziman, Phys. Rev. C **73**, 034601 (2006).
[15] E. D. Johnson, G. V. Rogachev, V. Z. Goldberg, S. Brown, D. Robson, A. M. Crisp, P. D. Cottle, C. Fu, J. Giles, B. W. Green, K. W. Kemper, K. Lee, B. T. Roeder, and R. E. Tribble, Eur. Phys. J. A **42**, 135 (2009).
[16] W. von Oertzen, T. Dorsch, H. G. Bohlen, R. Krücken, T. Faestermann, R. Hertenberger, T. Kokalova, M. Mahgoub, M. Milin, C. Wheldon, and H. F. Wirth, Eur. Phys. J. A **43**, 17 (2010).
[17] M. L. Avila, G. V. Rogachev, V. Z. Goldberg, E. D. Johnson, K. W. Kemper, Y. M. Tchuvil'sky, and A. S. Volya, Phys. Rev. C **90**, 024327 (2014).
[18] B. Yang, Y. L. Ye, J. Feng, C. J. Lin, H. M. Jia, Z. H. Li, J. L. Lou, Q. T. Li, Y. C. Ge, X. F. Yang, H. Hua, J. Li, H. L. Zang, Q. Liu, W. Jiang, C. G. Li, Y. Liu, Z. Q. Chen, H. Y. Wu, C. G. Wang *et al.*, Phys. Rev. C **99**, 064315 (2019).
[19] T. Sakuda, Prog. Theor. Phys. **57**, 855 (1977).
[20] T. Sakuda, S. Nagata, and F. Nemoto, Prog. Theor. Phys. **59**, 1543 (1978).
[21] H. J. Assenbaum, K. Langanke, and A. Weiguny, Z. Phys. A: At. Nucl. (1975) **318**, 35 (1984).
[22] D. Baye and P. Descouvemont, Phys. Lett. B **146**, 285 (1984).
[23] P. Descouvemont and D. Baye, Phys. Rev. C **31**, 2274 (1985).
[24] Y. Suzuki, A. Yamamoto, and K. Ikeda, Nucl. Phys. A **444**, 365 (1985).
[25] N. Furutachi, M. Kimura, A. Dote, Y. Kanada-En'yo, S. Oryu, A. Doté, Y. Kanada-En'yo, and S. Oryu, Prog. Theor. Phys. **119**, 403 (2008).
[26] T. Baba and M. Kimura, Phys. Rev. C **100**, 064311 (2019).
[27] F. Ajzenberg-Selove, Nucl. Phys. A **392**, 1 (1983).
[28] T. Kawabata, H. Akimune, H. Fujita, Y. Fujita, M. Fujiwara, K. Hara, K. Hatanaka, M. Itoh, Y. Kanada-En'yo, S. Kishi, K. Nakanishi, H. Sakaguchi, Y. Shimbara, A. Tamii, S. Terashima, M. Uchida, T. Wakasa, Y. Yasuda, H. Yoshida, and M. Yosoi, Phys. Lett. B **646**, 6 (2007).
[29] Y. Kanada-Enyo, Phys. Rev. C **75**, 024302 (2007).
[30] Y. Funaki, T. Yamada, H. Horiuchi, G. Röpke, P. Schuck, and A. Tohsaki, Phys. Rev. Lett. **101**, 082502 (2008).
[31] T. Yamada, Y. Funaki, H. Horiuchi, K. Ikeda, and A. Tohsaki, Prog. Theor. Phys. **120**, 1139 (2008).
[32] M. Ito, Phys. Rev. C **83**, 044319 (2011).
[33] T. Ichikawa, N. Itagaki, Y. Kanada-En'Yo, T. Kokalova, and W. Von Oertzen, Phys. Rev. C **86**, 031303(R) (2012).
[34] T. Yamada, Y. Funaki, T. Myo, H. Horiuchi, K. Ikeda, G. Röpke, P. Schuck, and A. Tohsaki, Phys. Rev. C **85**, 034315 (2012).
[35] Y. Kanada-En'Yo, Phys. Rev. C **89**, 024302 (2014).
[36] Z. H. Yang, Y. L. Ye, Z. H. Li, J. L. Lou, J. S. Wang, D. X. Jiang, Y. C. Ge, Q. T. Li, H. Hua, X. Q. Li, F. R. Xu, J. C. Pei, R. Qiao, H. B. You, H. Wang, Z. Y. Tian, K. A. Li, Y. L. Sun, H. N. Liu, J. Chen *et al.*, Phys. Rev. Lett. **112**, 162501 (2014).
[37] Y. Chiba and M. Kimura, Phys. Rev. C **91**, 061302(R) (2015).
[38] T. Yamada and Y. Funaki, Phys. Rev. C **92**, 034326 (2015).
[39] Y. Chiba, M. Kimura, and Y. Taniguchi, Phys. Rev. C **93**, 034319 (2016).
[40] Y. Kanada-En'yo, Phys. Rev. C **93**, 054307 (2016).
[41] B. Zhou, A. Tohsaki, H. Horiuchi, and Z. Ren, Phys. Rev. C **94**, 044319 (2016).

[42] Y. Chiba, Y. Taniguchi, and M. Kimura, Phys. Rev. C **95**, 044328 (2017).
[43] Y. Kanada-En'yo and Y. Shikata, Phys. Rev. C **100**, 014301 (2019).
[44] Y. Chiba and M. Kimura, Phys. Rev. C **101**, 024317 (2020).
[45] Y. Kanada-En'yo and K. Ogata, Phys. Rev. C **101**, 014317 (2020).
[46] J. Berger, M. Girod, and D. Gogny, Comput. Phys. Commun. **63**, 365 (1991).
[47] Y. Kanada-En'yo, M. Kimura, and H. Horiuchi, C. R. Phys. **4**, 497 (2003).
[48] M. Kimura, Phys. Rev. C **69**, 044319 (2004).
[49] Y. Kanada-En'yo, M. Kimura, and A. Ono, Prog. Theor. Exp. Phys. **2012**, 1A202 (2012).
[50] T. Baba and M. Kimura, Phys. Rev. C **94**, 044303 (2016).
[51] T. Baba and M. Kimura, Phys. Rev. C **95**, 064318 (2017).
[52] D. L. Hill and J. A. Wheeler, Phys. Rev. **89**, 1102 (1953).
[53] Y. Chiba and M. Kimura, Prog. Theor. Exp. Phys. **2017**, 053D01 (2017).
[54] M. Freer, R. R. Betts, and A. H. Wuosmaa, Nucl. Phys. A **587**, 36 (1995).
[55] S. Ohkubo and K. Yamashita, Phys. Rev. C **66**, 021301(R) (2002).
[56] M. Kimura and H. Horiuchi, Phys. Rev. C **69**, 051304(R) (2004).
[57] J. A. Maruhn, M. Kimura, S. Schramm, P.-G. G. Reinhard, H. Horiuchi, and A. Tohsaki, Phys. Rev. C **74**, 044311 (2006).
[58] T. Ichikawa, Y. Kanada-En'Yo, P. Möller, Y. Kanada-En'yo, and P. Möller, Phys. Rev. C **83**, 054319 (2011).
[59] J.-P. P. Ebran, E. Khan, T. Nikšić, and D. Vretenar, Phys. Rev. C **90**, 054329 (2014).
[60] D. Ray and A. V. Afanasjev, Phys. Rev. C **94**, 014310 (2016).
[61] J.-P. Ebran, E. Khan, T. Nikšić, and D. Vretenar, J. Phys. G **44**, 103001 (2017).
[62] N. Itagaki and S. Okabe, Phys. Rev. C **61**, 044306 (2000).
[63] W. von Oertzen, M. Freer, and Y. Kanada-En'yo, Phys. Rep. **432**, 43 (2006).
[64] M. Kimura, Phys. Rev. C **75**, 041302(R) (2007).
[65] T. Baba, Y. Chiba, and M. Kimura, Phys. Rev. C **90**, 064319 (2014).
[66] J. Li, Y. L. Ye, Z. H. Li, C. J. Lin, Q. T. Li, Y. C. Ge, J. L. Lou, Z. Y. Tian, W. Jiang, Z. H. Yang, J. Feng, P. J. Li, J. Chen, Q. Liu, H. L. Zang, B. Yang, Y. Zhang, Z. Q. Chen, Y. Liu, X. H. Sun *et al.*, Phys. Rev. C **95**, 021303(R) (2017).
[67] K. Ikeda, N. Takigawa, and H. Horiuchi, Prog. Theor. Phys. Suppl. **E68**, 464 (1968).